

QC
M 879.5
UE .U4
NE no.20
G.

ESSA Technical Memorandum NESCTM 20

U.S. DEPARTMENT OF COMMERCE
Environmental Science Services Administration
National Environmental Satellite Center

Mapping of Geostationary Satellite Pictures An Operational Experiment

R. C. DOOLITTLE, C. L. BRISTOR, and L. LAURITSON

Natio

eries

The National Environmental Satellite Center is responsible for the establishment and operation of the National Oceanic and Atmospheric Administration's Environmental Satellite System and the environmental satellite system for the Environmental Science Services Administration. The three principal offices of NESCTM are Operations, System Engineering, and Research. ESSA Technical Memoranda facilitate rapid distribution of material which may be preliminary in nature and which may be published formally elsewhere at a later date.

Memoranda in the NESCTM series are available from the Clearinghouse for Federal Scientific and Technical Information, U.S. Department of Commerce, Sills Bldg., 5285 Port Royal Road, Springfield, Va. 22151. Price: \$3.00 hard copy; \$0.65 microfiche. Order by accession number shown in parentheses at end of each entry.

- NESCTM 1 Publications by Staff Members, National Environmental Satellite Center and Final Reports on Contracts and Grants Sponsored by the National Environmental Satellite Center 1958-1966, March 1967. (PB-174 606)
- NESCTM 2 Publications by Staff Members, National Environmental Satellite Center and Final Reports on Contracts and Grants Sponsored by the National Environmental Satellite Center 1967. January 1968. (PB-177 189)
- NESCTM 3 Computer Processing of Satellite Cloud Pictures. C. L. Bristor, April 1968. (PB-178 319)
- NESCTM 4 Modification of the APT Ground Station Recorder for Increasing the Size of Recorded DRIR Data. Arthur S. Vossler, May 1968. (PB-179 322)
- NESCTM 5 NESCTM Digital Formatting System (DFS). Randall G. Hill, October 1968. (PB-180 588)
- NESCTM 6 Computer Processing of TOS Attitude Data. J. F. Gross, November 1968. (PB-182 125)
- NESCTM 7 The Improved TIROS Operational Satellite. Edward G. Albert, August 1968. (PB-180 766)
Supplement No. 1. Characteristics of Direct Scanning Radiometer Data, Edward G. Albert, April 1969. (PB-183 965)
- NESCTM 8 Operational Utilization of Upper Tropospheric Wind Estimates Based on Meteorological Satellite Photographs. Gilbert Jager, Walton A. Follansbee, and Vincent J. Oliver, October 1968. (PB-180 293)
- NESCTM 9 Meso-Scale Archive and Products of Digitized Video Data From ESSA Satellites. Arthur L. Booth and V. Ray Taylor, October 1968. (PB-180 294)
- NESCTM 10 Reserved.

(Continued on inside back cover)

U.S.

U.S. DEPARTMENT OF COMMERCE
Environmental Science Services Administration
National Environmental Satellite Center

ESSA Technical Memorandum NESCTM 20

MAPPING OF GEOSTATIONARY SATELLITE PICTURES
AN OPERATIONAL EXPERIMENT

R. C. Doolittle, C. L. Bristor and L. Lauritson

RECEIVED
U.S. DEPARTMENT OF COMMERCE
ENVIRONMENTAL SCIENCE SERVICES ADMINISTRATION



WASHINGTON, D.C.
March 1970

DC
8-1-5
U4

UDC 528.341:681.3:629.783:551.507.362.2:551.576(084.12)

528	Geodesy - Cartography
.341	Dynamic triangulation
681.3	Computers
629.78	Astronautics
.783	Satellites
551.5	Meteorology
.507.362.2	Meteorological satellites
.576	Clouds
(084.12)	Photographs

CONTENTS

	Page
ABSTRACT	1
I. INTRODUCTION	1
II. THE EXPERIMENTAL FACILITY	2
III. DIAGNOSTICS AND THE EVOLVING OPERATIONAL EXPERIMENT	3
IV. PICTURE PREPROCESSING AND RASTER NORMALIZATION	5
V. ATTITUDE DETERMINATION	8
VI. EARTH LOCATION AND THE MAPPED OUTPUT	11
VII. OUTLOOK AND RECOMMENDATIONS	12
ACKNOWLEDGMENT	16
REFERENCES	16
APPENDIX 1	A-1
APPENDIX 2	A-8

LIST OF FIGURES

<u>Number</u>	<u>Page</u>
1. ESSA Facility for ATS picture acquisition.....	17
2. Contoured ATS-I picture with line sector profiles.....	18
3. Horizon plots from ATS-I pictures showing raster skew and raster start (β) variability.....	19
4. Response histograms with early (left) and present response conditioning amplifier.....	20
5. Hundred line histograms of the right-hand plot in Figure 4. Only the earth viewing portions are included.....	21
6. Frame start detection monitor showing northern left horizon "notch" from Figure 2.....	22
7. December contoured image showing northward off-earth scan. Line graphics show the cyclic nature of noise in the space response.....	23
8. Enhanced landmark image sectors with coordinate identifica- tion for attitude evaluation.....	24
9. Automatic landmark recognition and matching procedure.....	25
10. ATS-I sample picture displayed on the photofacsimile recorder within the Digital Picture Terminal.....	26
11. Mercator mapped equivalent of the picture shown in Figure 10...	27
12. Polar stereographic sector images produced from Figure 10.....	28

MAPPING OF GEOSTATIONARY SATELLITE PICTURES - AN OPERATIONAL EXPERIMENT

R. C. Doelittle, G. L. Bristor and L. Lauritson

ABSTRACT

Spin scan cloud pictures from the ATS-I geostationary satellite were mapped for daily operational experimental use during the period from June to December 1969. The details of this continuing experiment are discussed herein. Computer programs are used, first to preprocess the digitized image data to produce a geometrically normalized picture, then to map the normalized image on Mercator or polar stereographic projections. In the summary, recommendations are made for operational processing of data from the projected operational geostationary satellite, and some speculative suggestions are advanced in regard to the possibilities for expanded computer processing in the future.

I. INTRODUCTION

Experimental processing of digital cloud image data from spin scan cloud cameras began with the launch of NASA's ATS-I satellite. Magnetic tapes, each containing one picture, were supplied to NESC from the Mojave ground facility. Eight thousand 8-bit samples for each of two thousand lines comprised each image tape recorded from the Spin Scan Cloud Camera (SSCC). A substantial software investment was made to explore the feasibility of automatically mapping the pictures and extracting quantitative information from them. Using horizon detection methods, the satellite spin axis was determined and pictures were mapped on a case study basis. Software performance on the CDC 6600 indicated the potential for a practical real-time operation.

Meanwhile, a feasibility study had begun toward the on-board digitizing of spin scan imagery from an operational geostationary satellite. As a result of this investigation, NESC obtained a ground-based Digital Picture Terminal (DPT) which processed ATS-I spin scan data from simulated on-board digitizing.

By mid-1968, NASA had completed its primary experimental mission with the ATS-I spacecraft, and discussions were under way toward a NESC real-time operational experiment using picture sequences. Lapse-time movies had

indicated the feasibility of obtaining wind estimates from cloud motions. Accordingly, receiver and antenna facilities were readied at the NESC Wallops Island facility, and the breadboard digitizing and "line stretching" unit was upgraded to operational quality. With computer interface provided, the DPT unit was installed at Suitland, and operational experimentation started in May 1969.

By June, earlier software packages had been modified and linked into a workable configuration, and picture mapping efforts had begun. This report describes the computerized aspects of this experiment with particular emphasis on the mapping operation. Problems encountered and results obtained are recorded for the 6-month period through December 1969. Finally, these experiences are summarized in the form of recommendations with respect to ESSA's projected Geostationary Operational Environmental Satellite (GOES) system.

II. THE EXPERIMENTAL FACILITY

Technical documentation (1) supplied with the hardware facility is paraphrased superficially in Figure 1. Only the primary logical functions are indicated. SSCC video and sun sensor signals received from the spacecraft are ingested and preprocessed in the Line Stretcher. Clocking pulses generated from the sun sensor response are utilized to trigger video sampling during the five percent earth traverse portion of each spin cycle. A separate sample rate controller then manages the digitizing process. Finally, the samples are played out at a slowed rate and released as a serial bit stream during the remaining portion of the spin cycle.

Because of bandwidth restrictions, only 2048 (6-bit) samples per scan line are presently being relayed to the Digital Picture Terminal at Suitland. A bit stream correlator detects implanted marker bits and thereby provides frame start and line synchronizing signals. The serial bit stream is then reformatted into individual samples, and the grey code, employed in the digitizer, is translated into standard binary sample counts. Photo recording employs a modulated beam which traces the image on film mounted on a screw drawn rotating drum. Alternately, the same image information can be passed to a small computer and stored on digital magnetic tape. In order to preserve software compatibility, this so-called "raw ingest tape" has been augmented to contain 4096 samples per scan line through duplication of each sample.

Added logic permits the small computer to drive the photo recorder for the display of digital material from any source. In this mode, the digital samples are again converted to a serial bit stream and photo recorded as though originating from the Line Stretcher.

III. DIAGNOSTICS AND THE EVOLVING OPERATIONAL EXPERIMENT

An earlier report (2) describes a substantial SSCC data processing activity, and subsequent interim reports (3) discuss alterations in the evolving effort. The operational aspects of the experiment have emphasized the value of diagnostic software. A variety of diagnostic tools, together with some discussion of picture signal attributes which prompted their adoption are presented in this section.

Figure 2 is a composite of two diagnostic tools. Using the raw digital tape from the Line Stretcher, an image is produced on a standard 18-inch, weather facsimile recorder. The melded grid identifies each hundredth line and each fiftieth sample. Response has been contoured using a three shade (grey, white, black) repeated combination.

The image provides assessment of picture quality from several standpoints. Presence of some retrace imagery (following the preceding picture) assures identification of the first scan line - a crucial requirement in the earth location process. Space viewing samples beyond both lateral horizons assures X-normalizing capability - the only means by which scan profiles can be related to the earth disk.

The contoured brightness topography permits image quality checks. Torn patterns have revealed line synchronizing problems, and extensive plateaus have flagged signal clipping at the bright extremity. Striations in the upper left space view portion of Figure 2 suggests a systematic noise component. Aberrations in the east horizon profile relate to a continuing exploration of a seeming anomaly in ATS-I signal response. Horizon profiles (insets) indicate the utility of a graphic tool which provides signal amplitude imagery as a function of an arbitrary (X in this case) coordinate. Tendency for response "overshoot" relates to picture coherence and the problem of picture realignment.

Figure 3 illustrates the raster coherence problem on the basis of horizon plots. The horizon profiles are obtained by plotting three-line average X-values. The bisector values are plotted on a greatly expanded X scale with ordinate markers (20L and 20R) indicating the span for forty samples. (Exact positioning of the center plot is not meaningful since it is subject to vagaries in detection of the starting reference line.) The upper plot involves the picture used in Figure 2, and the center plot is from a picture recorded 23 minutes later. Ideally, the center plot should be a vertical line. The overall skew of perhaps 40 samples suggests a systematic bias in raster synchronization. Sun pulse logic which triggers sampling at the proper spin phase angle (θ) and also corrects for changing sun angle during the twenty-minute picture scan period, characteristically yields such plots which slope downward to the right. The skew also varies from time to time - the lower plot, some six weeks after the upper pair, having a slope of perhaps 20 samples.

Deviations from the overall slope relate to the above mentioned overshoot problem. Eastern horizon detection is clearly influenced by the variability in brightness decay as the scan proceeds into the space scene. Inspection of many pictures indicates a systematic tendency for steeper westward slopes in bright image features and shallower slopes to the east. Summation of differences of adjacent scan sample pairs over large volumes of data substantiates this indication. When separated into low and high brightness groups, the brighter eastward slopes are significantly shallower than for the low brightness group. In seeking an explanation for this phenomenon, column averaging was performed to reveal a possible shift in response as the scan proceeds from west to east. Six columns were arranged symmetrically in three group clusters using a local noon image. The resulting 20 sample-by-1000-line column averages revealed no significant west to east trend. Since center plot anomalies, similar to those in Figure 3, have also been obtained with earlier NASA/Mojave tapes, there is some suggestion that the response problem may be in the satellite. No such perturbations have been revealed in similar plots from NASA/Rosman ATS-III tapes.

Response characteristics have been monitored using a variety of histograms. Whole raster response is indicated in two absolute histograms shown in Figure 4. For each (0-63) raw response value, the total population and percent occurrence is indicated. The distribution obtained with the earlier signal conditioning amplifier is shown (left) along with response from the revised amplifier presently in use.

The alteration has provided some improvement in sampling. Single values rarely occur with more than 4 percent frequency, whereas 10% occurrences were frequent in the earlier mode. These plots provide convenient checks for noise in the signal and identify problems in analog-to-digital (A/D) conversion. Figure 5 provides separate 100-line plots (starting at upper left and across) for the righthand case shown in Figure 4. Despite improvements in sampling with the amplifier change, there has been a shift and over-emphasis in the low responses. Since Figure 5 includes only earth viewing portions, it is apparent that all responses below a response of 15 in the total (right) histogram of Figure 4 reflect space response. The broad, secondary peak at the 3-response level was previously confined almost entirely within the zero response. Singular peaks suggest A/D converter problems. In Figure 5 - particularly the third from right (upper) and second from left (lower) - the plots suggest that the 32 response is exaggerated, and this view is strengthened by close examination of Figure 4. The more frequent 58 to 61 responses in Figure 4 (left) also suggests conversion problems. A ten-day averaging of 54 to 63 responses revealed a sharp preference for those values. With standard A/D converters, such anomalies are usually revealed as doubling or odd/even problems. Diagnosis of flaws with the present gray code converter will require more subtle analysis.

Software for frame start detection is monitored by graphic computer printout shown in Figure 6. Earlier experiences with the frame start marker (bit pattern) had shown that noise substantially weakened detection. Operational considerations later resulted in the use of the manual frame start option which further reduced ability to precisely identify the first picture scan line. Accordingly, horizon detection software was modified to find frame start by seeking the "notch" in the upper left horizon profile. With normal spin axis orientation, the limited north-south scan of ATS-I always provides such notches between the picture scan and the adjacent retrace cycles. The notch pattern of Figure 6 is a simple binary print of the brightness topography at the horizon detection threshold. This tool has provided insight into horizon detector design in the presence of noise.

A mid-October attitude maneuver was made in order to increase the northward extent of picture scan. The resulting scan beyond the earth's north limb (shown in Figure 7) forced use of the lower left notch in a revision of the frame start logic. Even short of off-earth scan, the southward march of the sun has obviously weakened utility of the upper left notch. The inset line profiles emphasize the cyclic nature of the space noise. The different noise pattern in the retrace sector suggests that the noise is a part of the signal arriving at the ground receiver. Any systematic noise injected by the ground equipment or transmission link would tend to form the same graphic pattern during both picture scan and retrace.

Extensive log sheets have been generated from diagnostic information supplied by the software discussed above. Emphasis has been placed on periodic review with subsequent modifications to eliminate pitfalls in the automated mapping effort. Further reference will be made to these tools in the following sections.

IV. PICTURE PREPROCESSING AND RASTER NORMALIZATION

The magnetic tape generated during the initial ingestion of digitized picture brightness at Suitland ("raw ingest tape") is not used directly in the mapping process for a number of reasons.

In the earth location calculations described in Section VI, latitude and longitude are computed for a rectangular array of "bench-mark points" in the picture, selected at regularly spaced scan line and sample numbers. Latitude and longitude are converted to map coordinates for the desired map projection and scale, and the map position of other image elements is obtained by interpolation. This procedure requires precise correlation between the arbitrarily selected bench-mark array and the scan line and sample numbers of the picture data to be mapped. The scan line in which the telescope is normal to the spin axis, and the mid-earth sample of this scan must be known relative to the bench-mark coordinates.

The raw ingest tape usually contains data from retrace scans preceding and following the picture to be mapped and the position of the mid-earth sample in each scan varies from picture to picture.

A preprocessing program has been written which searches the brightness data on the raw ingest tape to locate the edges of the earth disk on each line. This information is used in normalizing the raster in terms of frame and line start. A normalized data tape is then written which copies the raw ingest tape line-by-line, but eliminates retrace portions, and shifts the earth viewed portions of each scan to center them in the data format. The first data line record of the normalized tape corresponds to the maximum northward excursion of the telescope and the central record (line 1009 of the 2017 for a full picture) contains data taken with the telescope perpendicular to the spin axis. The central sample (2048) corresponds to the mid-earth position of the telescope.

In addition to the normalized picture data tape which is used as the basic input for mapping, a second tape is output which contains the sample numbers of the left and right edges of the earth disk for each line. The first file of this tape is formatted to produce a graphic record (Figure 3). A second file contains the data in digital form for input to one of the attitude determination programs described in the next section. There is also an option to output a normalized data tape formatted for a CRT display device. Details of the frame start and line start determination are described below.

Determination of Frame Start

Frame start and line start marker bits are included in a fixed position in a 120-bit preamble at the beginning of each picture data record on the raw ingest tape. Initially the preprocessing program relied upon a line-by-line test for the frame start marker bits. This procedure proved unreliable for several reasons and was replaced by detection of the horizon notch. (In some cases, more than one frame start marker was found. In others, the marker was not present, or could not be found because of garbled data or a shift in position of the marker bits from those tested. Finally, the marker when found was often several lines above or below the frame start scan indicated by earth edge data.)

With earth disk edge points provided, the tables of horizon sample numbers are examined to find the notch between the retrace scans and the first scan of the picture to be mapped and to determine the mid-earth sample number. Use of the upper horizon notch was reliable (and accurate to within 1 picture scan) where well defined. The previously discussed Figure 6, illustrates the northern horizon notch (maximum left earth edge sample number) for an ATS-I picture. However, after the attitude maneuver of November 8, 1969, the picture included the northern edge of the earth disk so that the notch widened into a gap, with the telescope seeing only space at its northward limit. In this situation the program erroneously located frame start at an earth edge above or below the gap.

Consequently, the logic was modified to find the notches at both top and bottom of the picture and to base frame start on the one closest to the midearth scan. (If the southern notch is selected, the starting scan number is obtained by subtracting 2016.)

Line Start Normalization

The constant shift to be applied to the earth sample population within the format of each line is the difference between the observed midearth sample number and the raster center (2048). The precision with which the mid-earth sample number can be found is dependent upon the detection of left and right edges of the earth disk, and is limited by noise in the space viewed portions of the scan.

The horizon detection logic is one of simple thresholding in which the digitized picture is searched, starting with space viewed portions of each line and working toward the picture center until brightness values exceeding an input threshold are found. This procedure works well in the absence of noise in the space viewed portions of the data and, in the most favorable cases, satisfactory results were obtained with the threshold set at 0 for space and 1 or greater for earth. (Three successive values of 1 or greater were required to avoid occasional isolated noise samples.) However, during the course of the operational experiment the data has become increasingly noisy, and the effect of the noise has been intensified following the mid-October amplifier alteration. At this writing, the threshold has been set at 16 or greater for earth, and 20 successive values above the threshold are set as a minimum to eliminate noise bursts. Use of a high threshold results in too small an earth population especially in scans at the upper and lower latitude limits of the picture where the illumination level is low.

The loss of accuracy in the position of the edge of the earth disk from use of a high threshold does not significantly affect the determination of frame start. However, the position of the midearth sample number is adversely affected, and the determination of spin axis attitude from horizons, described in section V below, requires the greatest accuracy obtainable. For this reason, logic has been added to the preprocessing program to examine the magnitude and frequency of noise samples in the space viewed portion at the left and right ends of each line. From the noise distribution, thresholds, and the number of successive samples above threshold required to reject noise bursts, are computed and used. This "dynamic thresholding" procedure has not worked well because the space population tested has been limited to the outermost 100 samples to avoid earth response, and because the noise encountered at the edges of the line is not representative of noise adjacent to the earth disk in much of the picture.

In order to gain stability in the mapping operation, the procedure now used for line start normalization is to average the left horizon sample number for 50 lines nearest to the disk center, as found with a threshold of 16. The shift applied is the difference between this average left horizon position and the hypothetical left edge of a centered earth disk with a sample population of 3800. (This value for the number of samples in the full earth disk is discussed below in connection with the horizon method of attitude determination.) In Section III mention was made of a systematic tendency for steeper westward slopes in bright image features and shallower slopes to the east. This lack of symmetry is also shown by the shift in mid-earth sample numbers with different thresholds. One picture was tested with thresholds of 4, 8, and 16. The threshold of 4 was too low and triggered by noise outside the left horizon too often to permit a valid average. The mid-earth position for the threshold of 16 was shifted by 5 samples to the left from that for the threshold of 8.

Bias in the centering of the normalized data tape, as indicated by the mapped output, is nearly constant and is compensated for by a change in the spin-component of the input camera-attitude in the earth location calculations.

V. ATTITUDE DETERMINATION

Earth location calculations described in Section VI compute the latitude and longitude corresponding to a given scan and sample number in the picture by intersecting the earth spheroid with a ray of known direction from the known position of the satellite. The direction of the ray is obtained in two steps. First direction cosines in a camera coordinate system are found from the image scan and sample numbers. These direction cosines are then converted into corresponding values in the geocentric coordinate system used for the earth spheroid by multiplication with an orientation matrix which relates the two sets of coordinate axes.

The attitude determination procedures described here find three angles required for computation of the orientation matrix: the right ascension and declination of a geocentric vector parallel to the satellite spin axis and the rotation about the spin axis from mid-earth to the center of the picture format. Two basically different approaches to attitude determination were developed during the course of the experiment. One makes use of both illuminated horizons in a picture taken near local noon; the other, of landmarks (well-defined coastline points) appearing in the picture. The program using the earth-edge position requires more computer time and storage, and is more vulnerable to noisy picture data than that using landmarks. It has not been used to provide the attitude input to the earth locator programs, but has provided useful information as to the incremental angular change along a scan (radians per sample) and the drift of the mid-earth sample position from top to bottom of a picture. It is potentially useful for a quick attitude determination immediately after a spacecraft attitude maneuver until landmark line and sample numbers can be determined. (An earlier horizon method (2) requires earth edge data from

a series of pictures and could not be used in this experiment because only one or two pictures per day were processed digitally.) A description of the method and some results obtained with it are contained in Appendix 1. The landmark approach was initially programmed using a conventional photogrammetric procedure (4), modified for the difference between the ordinary perspective view and the SSCC image geometry. This procedure requires three or more landmarks. Because of the scarcity of landmarks seen by the SSCC from the ATS-I satellite at 150° west longitude, a more sophisticated procedure requiring only 2 or more landmarks was developed by Mr. Dennis Phillips and this has been the primary source of attitude input to the earth locator programs.

The present method using recognizable land features is only semiautomated. Cloud-free, singular targets such as islands and coastline irregularities are detected by eye. Their picture coordinates are estimated within a sample or two with the aid of enhanced image sectors. A grid specifying line and sample number is melded with a picture sector which has been greatly expanded by replicating each sample on the CRT display raster. Gray scale enhancement is employed in order to emphasize coastline discontinuities and spatial smoothing is avoided so that eye discrimination is possible on an individual sample basis. Sample sectors are shown in Figure 8. Sector boundaries can be estimated under stable conditions since the normalized tape provides the data source. A family of such sector images is routinely obtained as Polaroid prints. The observed picture coordinates for known land features are utilized along with equivalent coordinates provided through a preliminary attitude estimate in order to arrive at the final calculated value (see Appendix 2).

Meanwhile, a substantial effort has been expended toward the automation of the above procedure through pattern recognition. The first step involves edge detection in order to generate a family of x, y points for each selected land feature. Although Laplacian and slope methods have been tried, most experimentation has been done using simple brightness thresholding. The latter is least costly in computer time but does demand signal stability. Since a local noon picture is used each day, this has not been a serious problem. Also, the brightness slice level is separately adjustable for each target sector.

Once edge points have been generated, there remains the automatic determination of the offset between the observed points and those generated from the attitude "first guess." Here, added pattern manipulation is utilized in order to reduce the search penalty in the matching process. Figure 9 will help explain the process. The family of boxed figures (upper) represent the imaged land feature locations. The known locations are transformed into picture coordinates through the initial attitude estimate. The i, j coordinates are actually "normalized" equivalents of the x, y image coordinates. This transformation is done in order to provide a standardized array for the matching logic program. Since discontinuities are introduced into the array by the scarcity of measured points (heavy boxes), a realm of contiguous elements has been created by replication.

Seeking a match between the "plated" point realms now becomes a simpler process. At present, this logic makes Boolean match tests until at least

75% overlap is found between the two realms.

An average distance between corresponding points is applied as an adjustment to the image position of the known landmark features and another match is made. This continues until a minimum variance of the distance is found.

There may be erroneous "landmarks", i.e. cloud edges within the image realm. Supposedly, the landmarks to be matched will be distinct from the erroneous values. The best fit, i.e. smallest variance of the distance will occur when the proper landmarks are matched.

In the landmark-poor Pacific scene of ATS-I, some thought has been given to the use of island clusters as landmarks. The islands in a geographic sector—even if visible only through convective or orographic clouds which they support—would be expected to create a unique point pattern. A brightness slice through a companion section of the ambient picture might additionally contain cloud streets arising from the island cloud systems. Even so, the matching procedure might operate. A preliminary investigation was conducted in order to explore possibilities of such a technique. Using mercator mapped ESSA 9 imagery, the mid-Pacific island scene was examined and some multiday computer compositing was done. Apart from Hawaii (routinely used), New Caledonia and Fiji sector offered promising possibilities. Although further work is planned, island landmark utility may well remain somewhat marginal until the higher resolution GOES imagery becomes available.

Several methods for determining the attitude of ATS spacecraft are described in Reference (3). One of these which has been programmed for computer processing makes use of antenna polarization and sun data (Reference 3, Volume 2, Sections 5.1.3 and 5.3.3) and is reported to have an estimated accuracy of 0.5 to 1.0 degrees of great circle arc. This is sufficient for some spacecraft management purposes, but inadequate for mapping. Others (Reference 3, Volume 6, Section 8.1.5 and Reference 5) which utilize earth edge data from one or more pictures obtain attitude estimates with standard deviations ranging from less than 0.1 degrees of great circle arc for a single picture to 0.02 degrees or less using combined data from several pictures. The methods developed at NESC for the mapping experiment are comparable in accuracy to the latter figure and have operational advantages in that they do not require the processing of several pictures in a sequence, and do not require prior knowledge of the beta dot setting used in the picture processing at the data acquisition station. For this experiment, their use was made practical by the stability of the spin axis orientation between attitude maneuvers which permitted use of the same attitude for several days while landmark picture coordinates were being obtained for a new determination. For any full fledged mapping operation using pictures from a geostationary satellite, an attempt should be made to determine spin axis drift rates in right ascension and declination. If these drift rates are stable and not insignificant, mapping accuracy could be improved by using predicted attitudes.

VI. EARTH LOCATION AND THE MAPPED OUTPUT

With normalized image tape, orbital elements, spin axis attitude and picture start time, the earth location calculations can begin. Software used is an outgrowth of similar programs which support the ESSA vidicon image mapping operation (7). Modifications are similar to those employed in mapping Nimbus scanning radiometer data. Latitude/longitude locations are computed for a sparse array of image elements. By arranging this array in binary increments, interpolative logic can be programmed without using costly multiply instructions. Accordingly, the lines and samples are spaced 32 elements apart - a sparsity which still permits location of intervening samples by simple linear interpolation. The open array latitude/longitude points are converted to square mesh map overlay coordinates before the interpolative process begins.

For Mercator mapping, the map mesh size provides 25.6 elements per geocentric degree of arc. Approximately 100 degrees of arc are mapped in both E-W and N-S directions. Because of N-S elongation of the Mercator map geometry, the resulting array consists of 2550 x 2968 elements. The mesh size is chosen for convenience in scaling certain facsimile transmission products and because the line-to-line camera resolution is also approximated. Even so, picture sample population is inadequate in foreshortened edge areas - particularly in the high-latitude regions where map squares represent smaller areas on earth. A sample picture is presented - first, recorded directly in its original perspective (Figure 10) and then in Mercator mapped form (Figure 11). Two images, adjacent in time, are presently being mapped on a daily basis with image products being distributed on a real-time basis.

Midlatitude sectors are also being mapped in polar stereographic form on a single-picture-per-day basis. Here the map array is based upon the standard numerical prediction grid with each large square subdivided into a 64 x 64 fine mesh. Average resolution for this array is somewhat greater than two miles. Samples from the same source image are shown in Figure 12.

All mapped imagery is held in reserved disk space on the CDC 6600 for image product extraction and other quantitative product experimentation.

Each day, three archival tape files (two reels) are produced containing the two Mercator mapped images and the single picture polar sector pairs. Adequate documentation is provided for future experimental use.

The entire diagnostic and mapping operation represents a substantial daily computing investment. Beyond the minor commitment for preliminaries, each Mercator mapping requires 16 minutes of computer time. Because of the approximate alignment between raw image scan line data and the map mesh array, little can be done to improve the efficiency of this program. However, the polar sector arrays are not aligned with the scan raster and special care is required in reducing semiredundant disk accesses. Earlier versions requiring over twenty minutes per polar sector mapping have now been reduced to ten minutes.

Mention should be made of efforts toward brightness normalization of the mapped image since many projected uses would be strengthened. Although not

yet a part of the daily routine, software is in test for this purpose. First versions have altered raw response as a simple isotropic function of the solar zenith angle. Such normalizing creates brightness discontinuities unless care is taken to proceed in smaller horizontal steps where the correction profile is steep. Corrections stepped at varying horizontal intervals are being tested in order to avoid such discontinuities.

Accuracy in the mapping operation continues to be less than that desirable for a routine operation. Horizon detection problems and the dearth of landmarks in the Pacific are prime contributing factors. For automatic cloud displacement determination using adjacent picture pairs, the relative mapping error is more critical. Under normal conditions, a cross-correlation technique usually indicates a relative error in the order of 2-6 picture elements in mapping the Baja California coast. The absolute error may be 30-60 miles. Operational utility is maintained under such conditions since cloud motions are expressed as average displacements using 120-150 mile sectors.

A variety of factors have influenced the operational experiment. Receipt of proper digitized pictures has been adversely influenced by: higher priority demands upon the ATS-I spacecraft, ground receiver/Line Stretcher problems, and problems with the communication line or with the DPT. The intent has been to retain one digital picture tape per day during the June - October period and two per day thereafter. The percent of successful days, overall, is 44. From November 1 through December 15, percent success involving two tapes per day was 71.

Similarly, the goal has been daily mapped imagery, first on a one-per-day basis and, since November 1, two per day. Additional problems arise here. Operable software fails with changing signal conditions and alterations must be made. Human errors occasionally occur in preparation of parameter cards and in the proper sequencing of computer jobs. Large-scale computer outages - both from computer hardware and site (power and air conditioning) problems - have also been responsible for substantial contributions to the mapping problems. From a marginal beginning, single picture mapping is now adequate in about 70% of the cases with proper input tapes. For days with pairs of input tapes, a mapped pair is usable for cloud motion computation only 50% of the time.

VII. OUTLOOK AND RECOMMENDATIONS

Although the operational experiment is continuing and has not yet been extended to cover the ATS-III satellite, experiences thus far have provided considerable insight and have generated opinions concerning the necessary attributes for the projected GOES system. The following paragraphs, therefore, are phrased as suggestions and recommendations toward a stable operational system for the mid-seventies.

Properties of the Imaging Signals

A request that sensor response be retained to a maximum degree with minimum

noise is, of course, axiomatic and yet it bears discussion. With scanning provided by the spinning spacecraft, referencing of the raster to the earth remains a crucial problem in horizon detection. Experience with horizon scanners on TIROS spacecraft suggests that the most meaningful portion of the profile for horizon detection is the low response "knee" which is generated as the sensor first sees the earth. Noise must, therefore, be minimized, particularly in the low-response range. Also, signal path limits should include healthy margins because of uncertainties in the definition of information content. Noise equivalent temperature differences, or analogous specifications for visual channel sensors, tend to ignore the possibilities for information extraction through spatial filters. Many examples exist in the pattern recognition literature which illustrate the extraction of image edge features from extremely noisy data. In some applications, gradient detection is more important than absolute signal level determination. Bandwidth restrictions from the satellite and restricted count ranges in digital sampling are, therefore, to be avoided if possible.

Picture Raster Determination

Apart from "X-normalization" of the scan line with respect to the earth, other important factors remain. The mentioned problem with first line identification and the ability to maintain line count in the presence of sporadic noise should be stressed. One suggestion involves provision for a line number "signature" affixed to each position of the stepping mirror.

Precise knowledge of the sample population per degree of spin phase angle is also most important. With projected half mile earth sampling, improvement in satellite spin period determination is indicated and, in this connection, suggestions for sharpening of the sun pulse are in order. Whether controlled by sun pulses or by separate oscillator, the sample rate controller is, of course, an equally critical factor.

Picture horizon center plots also suggest need for improvement in line-to-line raster coherence. Bias in such plots indicate imperfections in the techniques used in correcting for changing sun angle during the picture scan.

The purpose here is to lend support to the variety of suggestions for improved raster determination and improved stability. To the extent that such inputs must be deduced through horizon detection techniques, the alternate use of horizon information for attitude determination is thereby weakened.

Attitude and Station Determination

Improvements in signal quality and raster precision would doubtless improve the determination of spin axis orientation by horizon detection techniques.

Although the landmark technique will be favored in the target-rich Western Hemisphere location projected for the first operational spacecraft, there will likely be need for both techniques as the program expands. The likelihood also exists for experimental operations with the ATS-III spacecraft. Without the signal "overshoot" problem and with more landmarks, improved

performance may be expected from both techniques.

Attitude determination by means of star mapping has been suggested. If adequate raster stability can be achieved and if dynamic range for earth sensing is adequate for star sensing, then this suggestion would seem to require only simple spin phase angle offset in order to obtain an adequate star map. Again, raster coherence is important.

The mapping experience, thus far, provides little evidence regarding the adequacy of present satellite position determination. Orbital elements provided from data supplied by the NASA ranging network appear to be adequate within present attitude and raster error constraints. Redundant mapping with deliberate 30-minute timing errors (both plus and minus) yielded appreciably degraded results.

Mention should be made of preliminary investigations into the feasibility of using landmarks for both attitude and position determination (8). Without an inclined orbit, the techniques tested appear to show promise for landmark-rich areas. More exhaustive study is indicated - perhaps also considering ground based laser targets and/or star map inputs - before any assertion could be made toward the substitution of such techniques in lieu of a ranging network.

Ground Station Facilities

Although the present Line Stretcher and DPT equipment are providing a valuable experience base, they are also serving to focus attention in the areas which weaken a routine operation.

Raster skew (the beta dot problem) has been discussed earlier. Although horizon center plots are subject to illumination deficiencies and vagaries of sensor response (overshoot), there appears to be a preponderant indication that the raster is skewed. The amount of skew seems to vary from 1% to perhaps 2½%, suggesting that hardware logic may not be performing within design limits.

While the beta dot adjustment is automatic, reversion to hand control is not necessarily the desirable alternate since raster start (beta), as a manual adjustment, has also created problems. Although substantial variations in raster start settings (Figure 3) are infrequent, actual horizon clipping can occur. Ideally, a more precise control would not only improve operational stability but would also permit reduction in waste space sampling.

The mentioned analog-to-digital converter imperfections introduce added signal contamination. Because of the experimental constraint for onboard digitizing, the present A/D converter was understandably built without provision for manual adjustment. For future systems, there is obvious need for improvement.

Suggestion has been made that a future ground system be designed with a fast general purpose computer providing primary line stretcher functions. With internal clocking of elapsed time between sun pulses, more sophisticated

treatment of anomalous spin periods could result in a better controlled raster. The beta dot offset (through a table lookup) could easily be tuned to eliminate bias. An appreciable number of secondary advantages would likely accrue. Considering the potential diagnostic assistance, the local option for digital tape buffering, picture gridding, etc., investigation of this mode versus Line Stretcher enhancement through augmented special equipment design would seem worthwhile. Ideally, the incoming signal would be received at the central computing and data using facility.

Large-Scale Computer Support

A predominant portion of the problem in routine mapping of picture pairs has, thus far, involved the large scale computer. Although further optimization of the operational software is indicated, there does not appear to be adequate dedication of the large scale facility to this mission. As operation of the dual large-scale facility is optimized, this situation is expected to improve.

Since faster, large-scale computers are now becoming available, it is tempting to suggest an expanded computer role for the mid-1970's operation. This operating mode would combine present loop movie hand analysis procedures and projected semiautomated video tape techniques along with the computer mapping approach.

At least two vendors now offer computers with five-fold increases in high-speed memory and in random access auxiliary (disk) memory. With 4-6 fold central processor throughput speed and high speed channels, such a facility would permit real-time mapping of an entire picture sequence for hand analysis as well as for further automated treatment.

Such a system would have many advantages. Apart from translational and rotational corrections, the mapping would remove all deformational distortions. Brightness normalization, enhancement, and local sector treatments would also be possible. With proper on-line CRT display, the beginning efforts toward automatic cloud motion determination could be tempered by human judgment. Those human inputs which became most objectively defined could then be automated in a gradual, evolutionary process. Such an operation would, of course, demand an adequately dedicated large-scale computing resource.

In summary, the operational experiment has been a most valuable experience thus far. Periods of stable operation indicate the potential for the future GOES system. The briefly mentioned automatic wind extraction effort is being tested with promising indications. Invariably, suggestions for the future focus on flaws, but detection of areas where improvement is indicated is one of the prime purposes of such an experiment. The only intent is to capitalize on present experiences toward improvement in the projected operational system.

ACKNOWLEDGMENT

This report summarizes an activity which includes the work of many of our colleagues. Special recognition is due Mr. D. Phillips who returned to graduate school before making formal report of his original work on the automatic determination of attitude from landmarks.

REFERENCES

1. Anon., "ESSA Digital Synchronizer and Line Stretcher" and "ESSA Digital Picture Terminal," Hughes Aircraft Company Final Reports for NESC under ESSA Contracts No. E-278-68 and No. E-185-67 (N), January 1969.
2. Whitney, M. B. Jr., R. C. Doolittle and B. Goddard, "Processing and Display Experiments Using Digitized ATS-I Spin Scan Camera Data," ESSA Technical Report NESC-44, April 1968.
3. Anon., "Applications Technology Satellite Technical Data Report," NASA ATS Program (updated monthly), March 1967.
4. Anon., "Manual of Photogrammetry," 3rd edition, Vol. 1, page 39, American Society of Photogrammetry, Falls Church, Va., 1965.
5. Anon., "ATS-III SSCC Data Reduction and Analysis Final Report," prepared for NASA under contract No. NAS 5-10217 by Westinghouse Electric Corporation/Defense Analysis Center, Baltimore, Md., April 1969.
6. Gross, J. F., "Computer Processing of TOS Attitude Data," ESSA Technical Memorandum NESCTM-6, November 1968.
7. Bristor, C. L., W. M. Callicott and R. E. Bradford, "Operational Processing of Satellite Cloud Pictures by Computer," Monthly Weather Review, Vol. 94, No. 8, 1966.
8. Dambeck, W., "Geostationary Satellite Position and Attitude Determination Using Picture Landmarks," ESSA Technical Memorandum NESCTM-21, (in preparation).

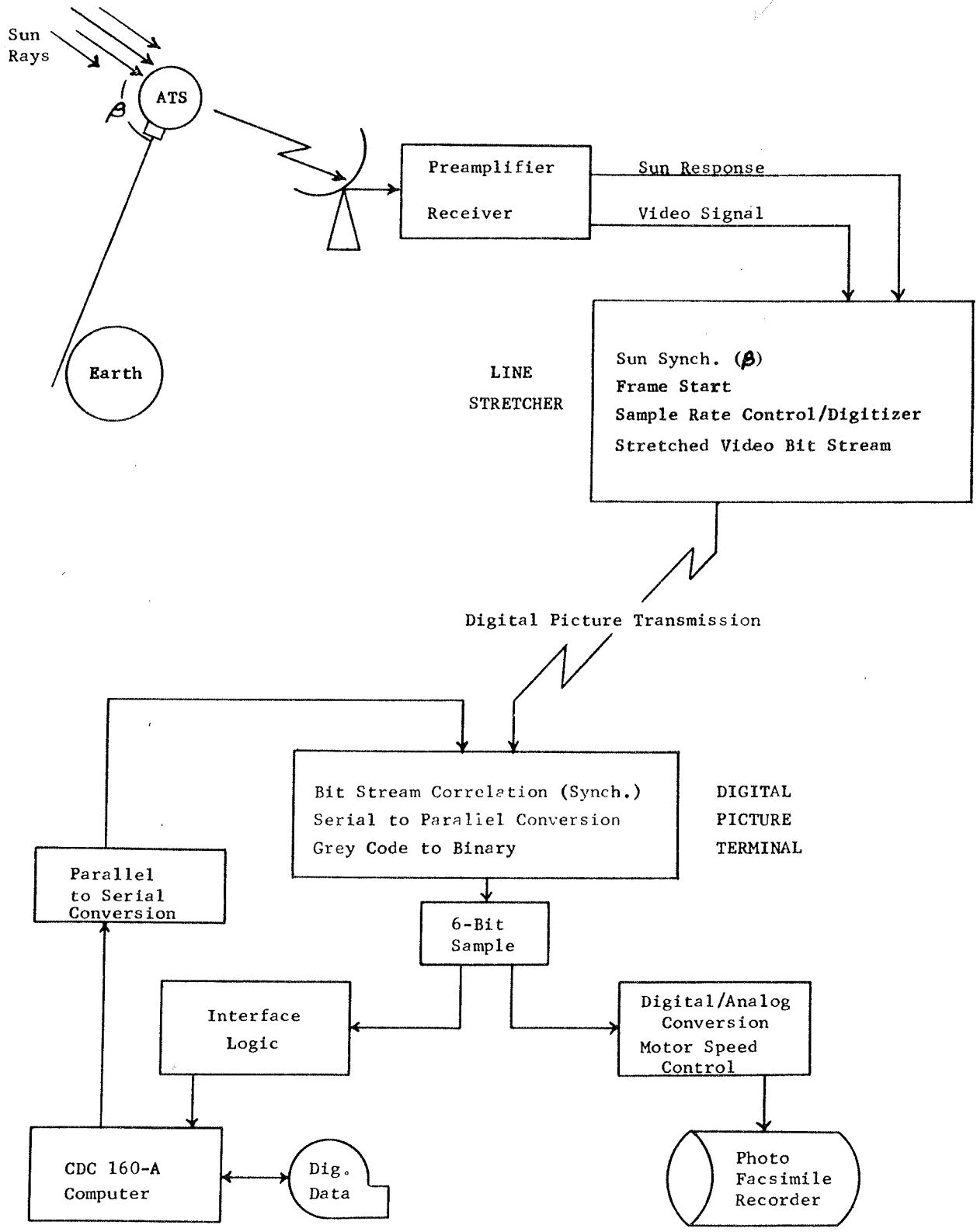


Figure 1. ESSA Facility for ATS picture acquisition.

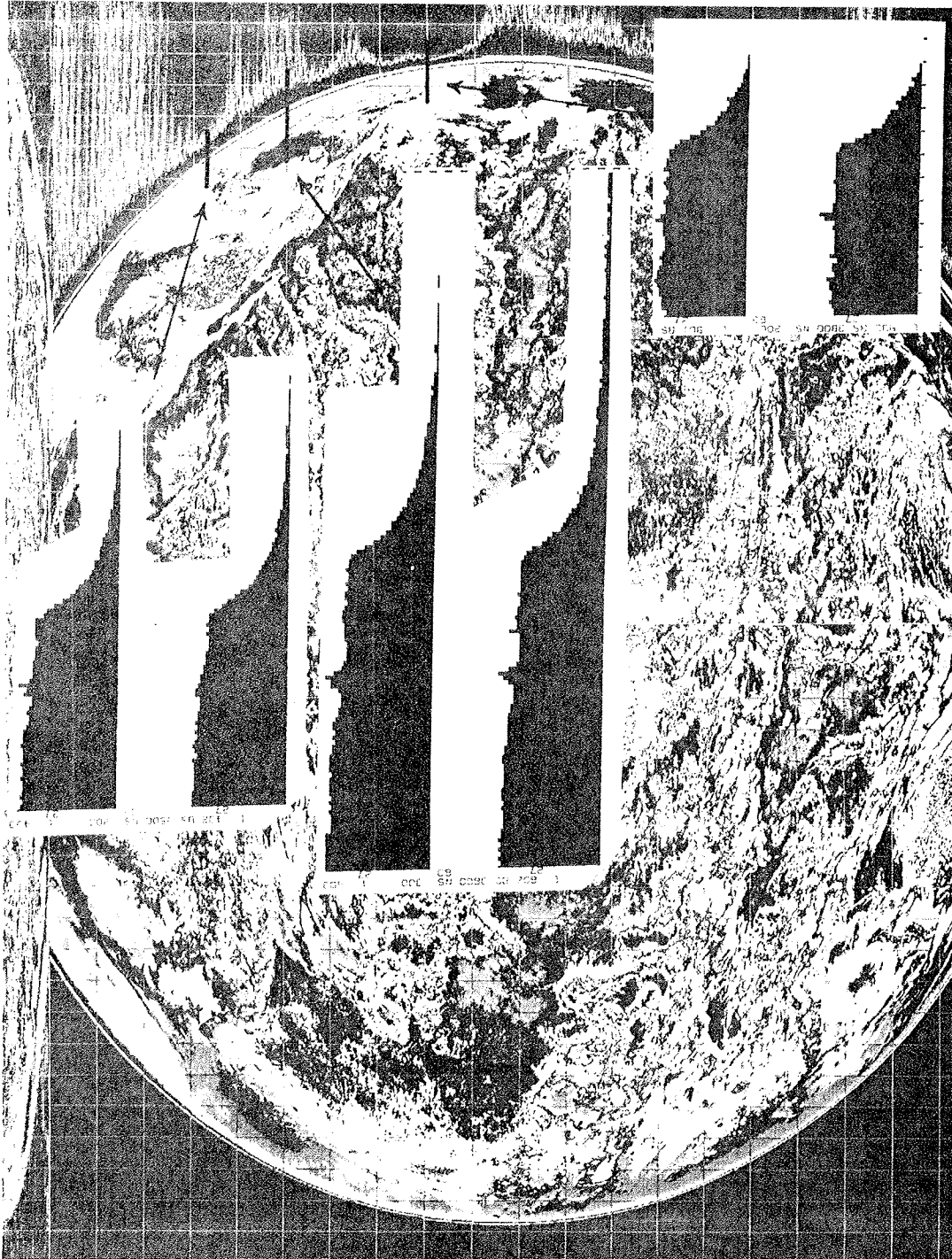


Figure 2. Contoured ATS-I picture with line sector profiles.

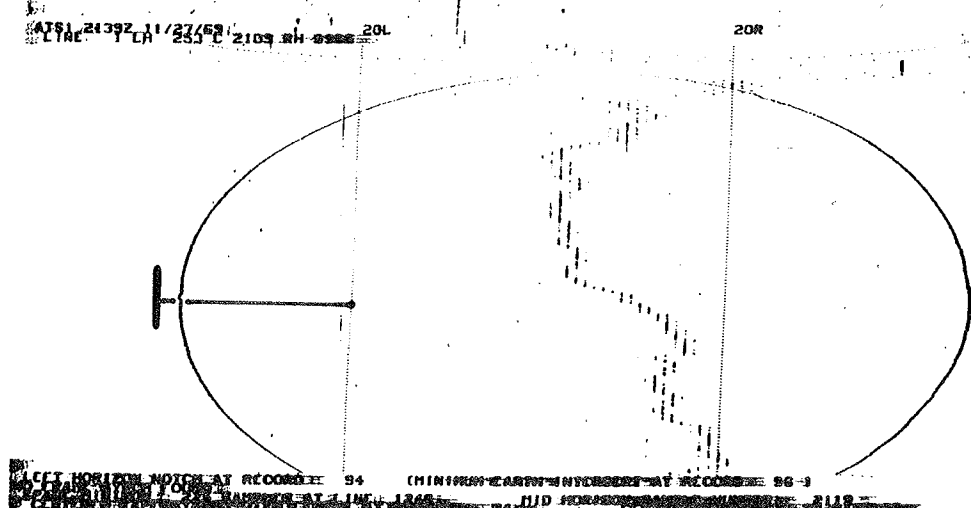
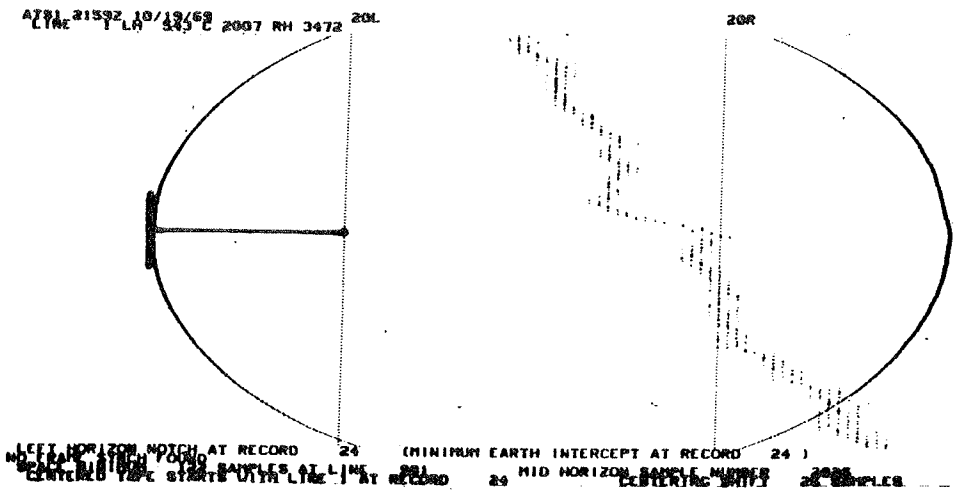
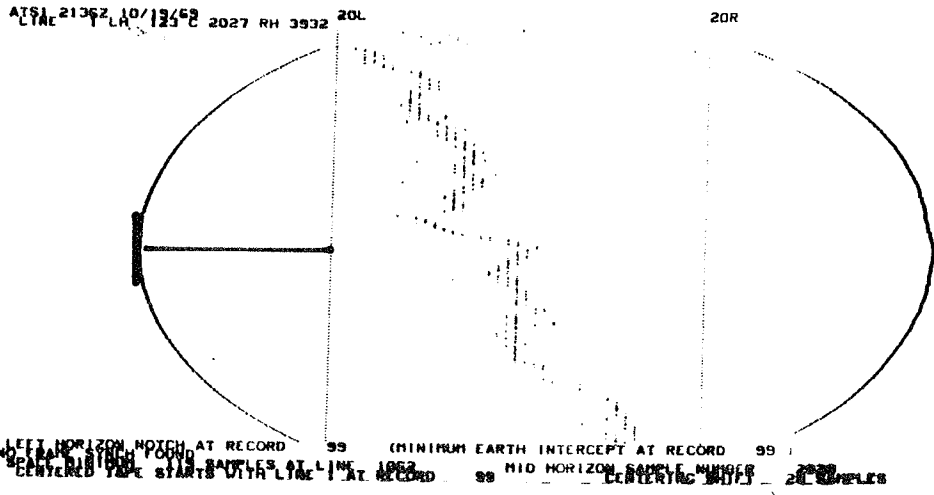


Figure 3. Horizon plots from ATS-I pictures showing raster skew and raster start (β) variability.

ATSI 69 07 03 2154Z

ATSI 2155Z 10/27/69

Index	Value	Count	Percentage
0	721071	*****	15.02
1	11883		.25
2	50779	**	1.06
3	437729	*****	9.12
4	541016	*****	11.27
5	419105	*****	8.73
6	322730	*****	6.72
7	291042	*****	6.06
8	220669	*****	4.60
9	174506	*****	3.64
10	147292	*****	3.07
11	127459	****	2.66
12	112844	****	2.35
13	97651	****	2.03
14	88859	****	1.85
15	99764	****	2.08
16	80398	***	1.67
17	67663	**	1.41
18	63043	**	1.31
19	61004	**	1.27
20	56474	**	1.18
21	54185	**	1.13
22	52012	**	1.08
23	54435	**	1.13
24	53184	**	1.11
25	43321	**	.90
26	40538	**	.84
27	37931	**	.79
28	35442	*	.74
29	31876	*	.66
30	27032	*	.56
31	21139	*	.44
32	22959	*	.48
33	18938	*	.39
34	17625	*	.37
35	16250	*	.34
36	14221	*	.30
37	12206	*	.25
38	9578		.20
39	8898		.19
40	7214		.15
41	6023		.13
42	5092		.11
43	4466		.09
44	3260		.07
45	2264		.05
46	1539		.03
47	1203		.03
48	821		.02
49	380		.01
50	376		.01
51	496		.01
52	436		.01
53	220		.00
54	0		0.00
55	16		.00
56	9		.00
57	1	VALUE, COUNT, BARGRAPH	.00
58	291		.01
59	398		.01
60	336		.01
61	381		.01
62	9		.00
63	18		.00

PERCENTAGE 0 5 10 15
FREQUENCY DISTRIBUTION VRS DIGITAL COUNT

Index	Value	Count	Percentage
0	801797	*****	9.71
1	19888		.24
2	81700	**	.99
3	409116	*****	4.95
4	274406	*****	3.32
5	36044	*	.44
6	16618		.20
7	12832		.16
8	10994		.13
9	6660		.08
10	7768		.09
11	5462		.07
12	5186		.06
13	4824		.06
14	4796		.06
15	6222		.08
16	5392		.07
17	7738		.09
18	20684	*	.25
19	46103	*	.56
20	86576	**	1.05
21	147938	****	1.79
22	199349	****	2.41
23	248456	*****	3.01
24	285996	*****	3.46
25	274818	*****	3.33
26	299282	*****	3.62
27	301284	*****	3.65
28	293488	*****	3.55
29	288242	*****	3.49
30	285416	*****	3.46
31	253916	*****	3.07
32	304520	*****	3.69
33	260566	*****	3.16
34	252946	*****	3.06
35	236962	*****	2.87
36	222262	*****	2.69
37	218962	*****	2.65
38	219966	*****	2.66
39	239990	*****	2.91
40	217044	*****	2.63
41	192028	*****	2.33
42	175504	****	2.13
43	154320	****	1.87
44	131128	***	1.59
45	112034	**	1.36
46	101112	**	1.22
47	95386	**	1.16
48	80474	**	.97
49	48402	*	.59
50	42203	*	.51
51	38212	*	.46
52	33048	*	.40
53	27964	*	.34
54	24124	*	.29
55	22414	*	.27
56	17190		.21
57	11392		.14
58	9410	VALUE, COUNT, BARGRAPH	.11
59	8072		.10
60	5616		.07
61	3576		.04
62	1666		.02
63	114		.00

PERCENTAGE 0 5 10
FREQUENCY DISTRIBUTION VRS DIGITAL COUNT

Figure 4. Response histograms with early (left) and present response conditioning amplifier. In each case the 0-63 response scale is shown at the left with corresponding population and percent occurrence indicated to the right.

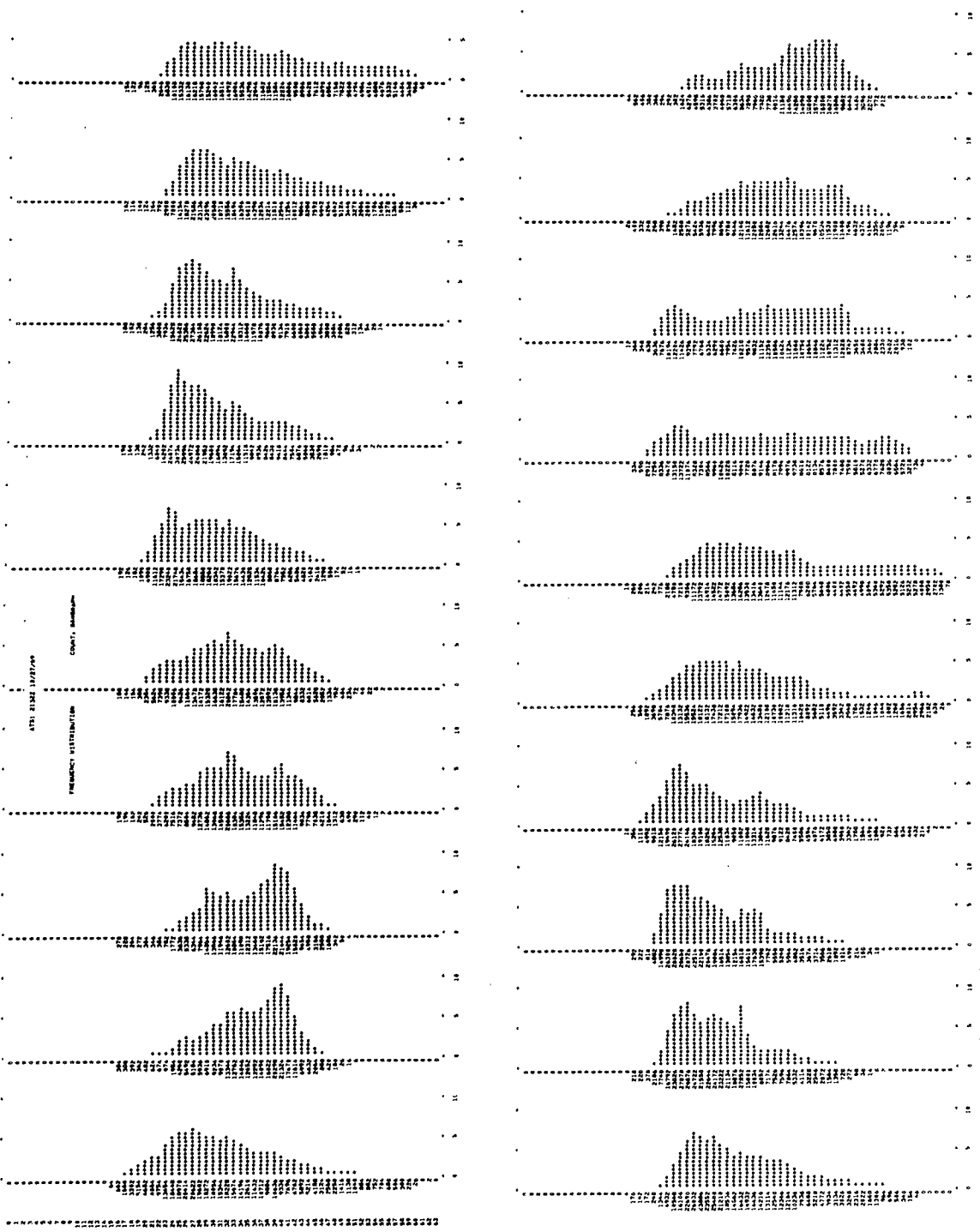


Figure 5. Hundred-line histograms of the right-hand plot in Figure 4. Only the earth viewing portions are included.

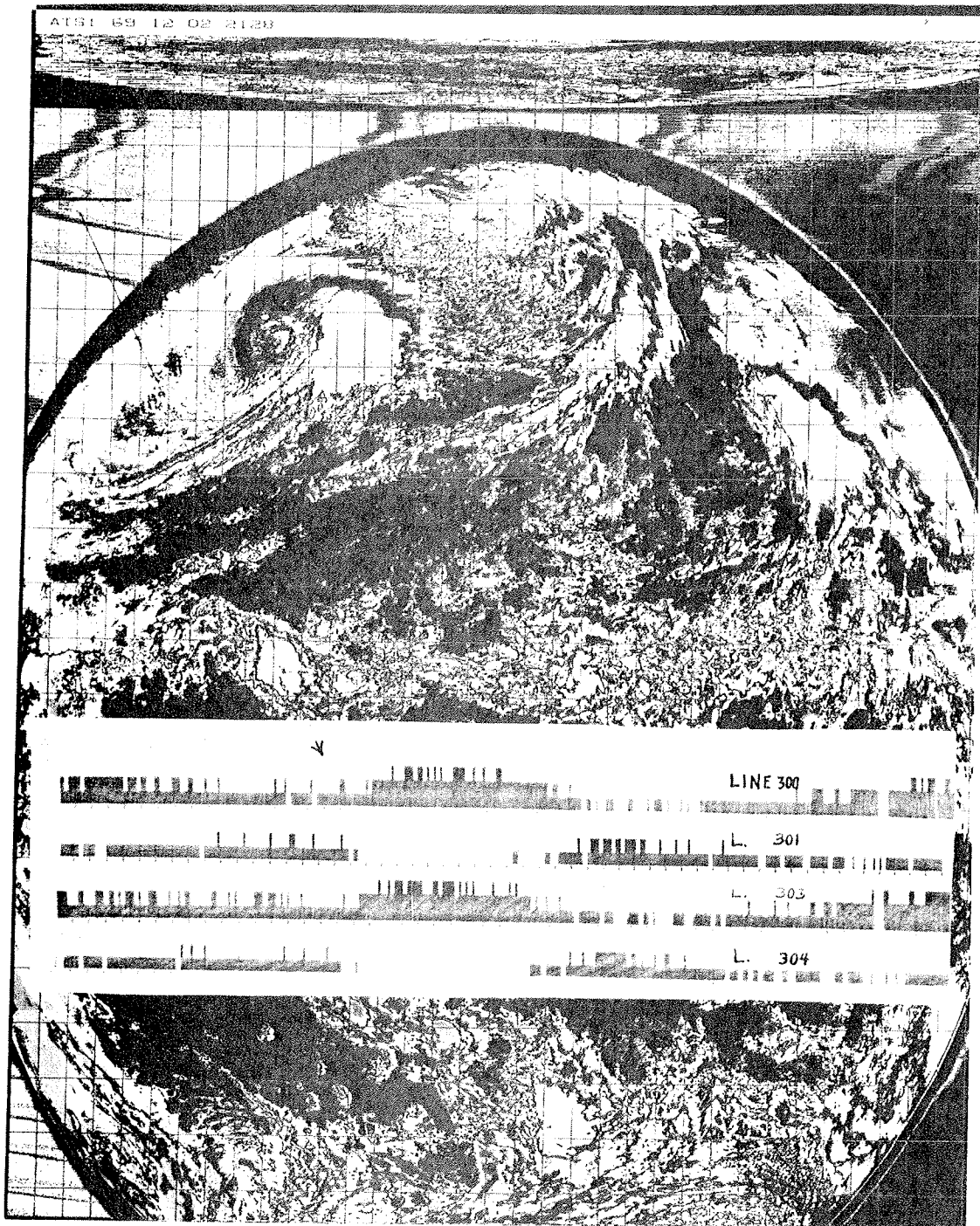


Figure 7. December contoured image showing northward off-earth scan. Line graphics show the cyclic nature of noise in the space response.

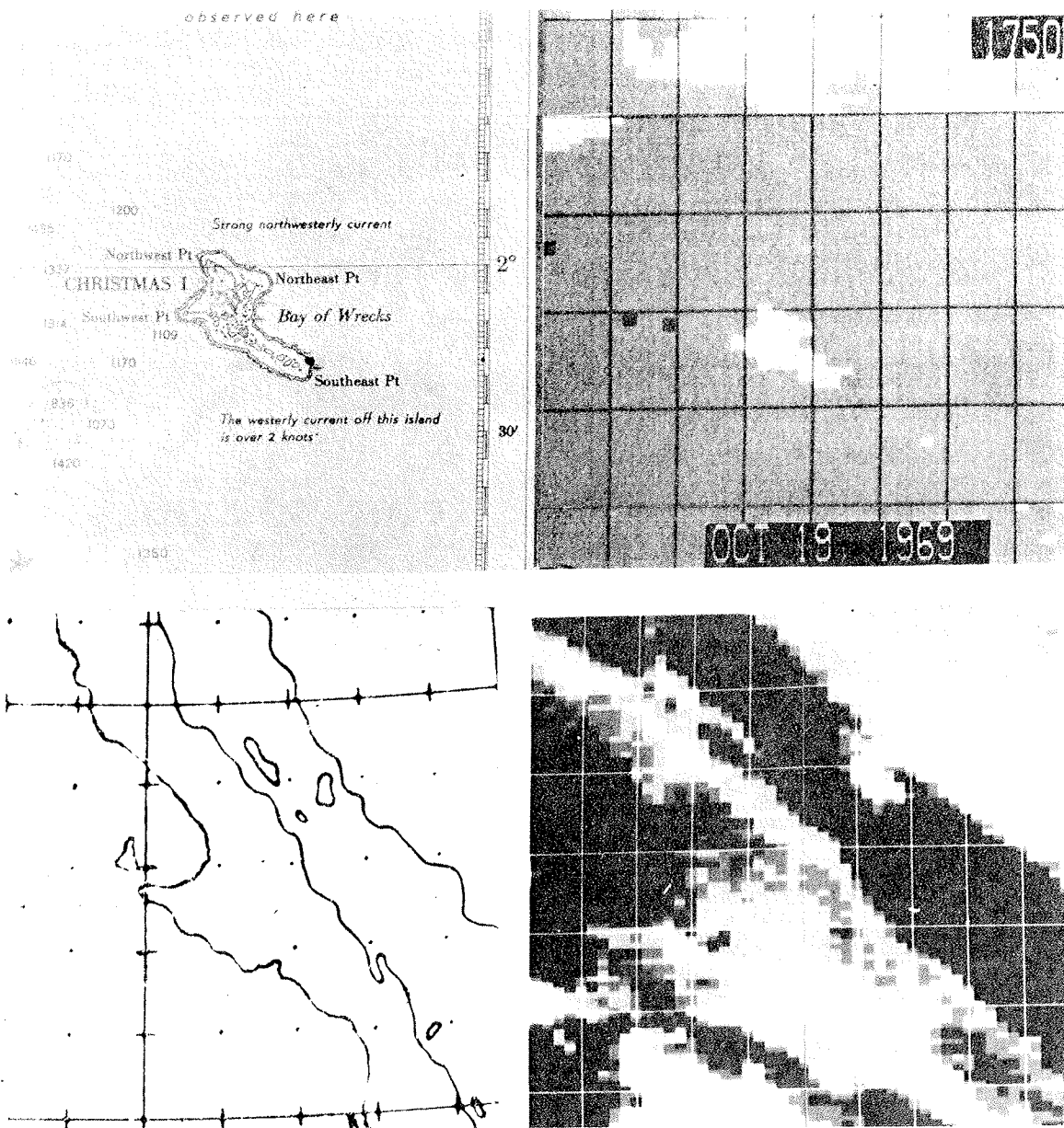


Figure 8. Enhanced landmark image sectors with coordinate identification for attitude evaluation.

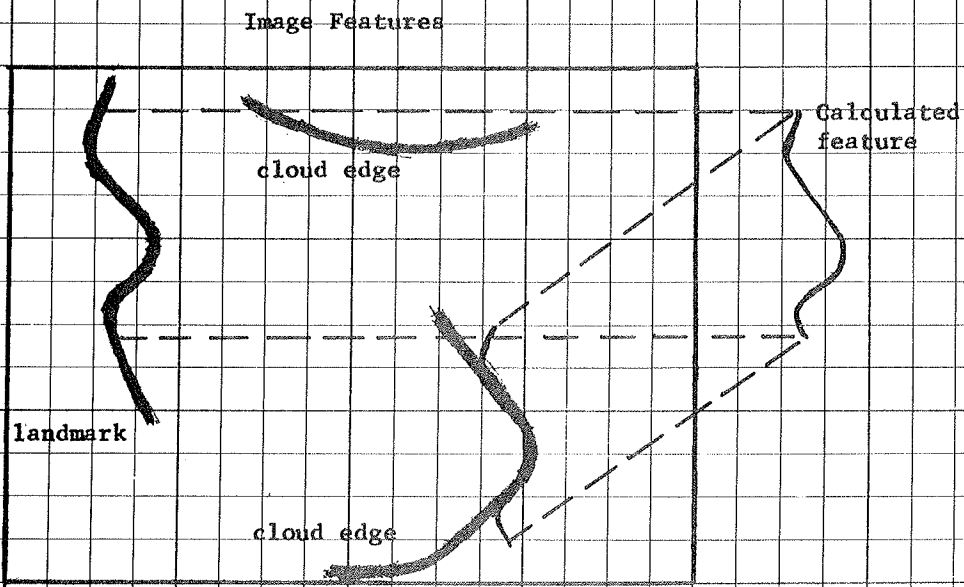
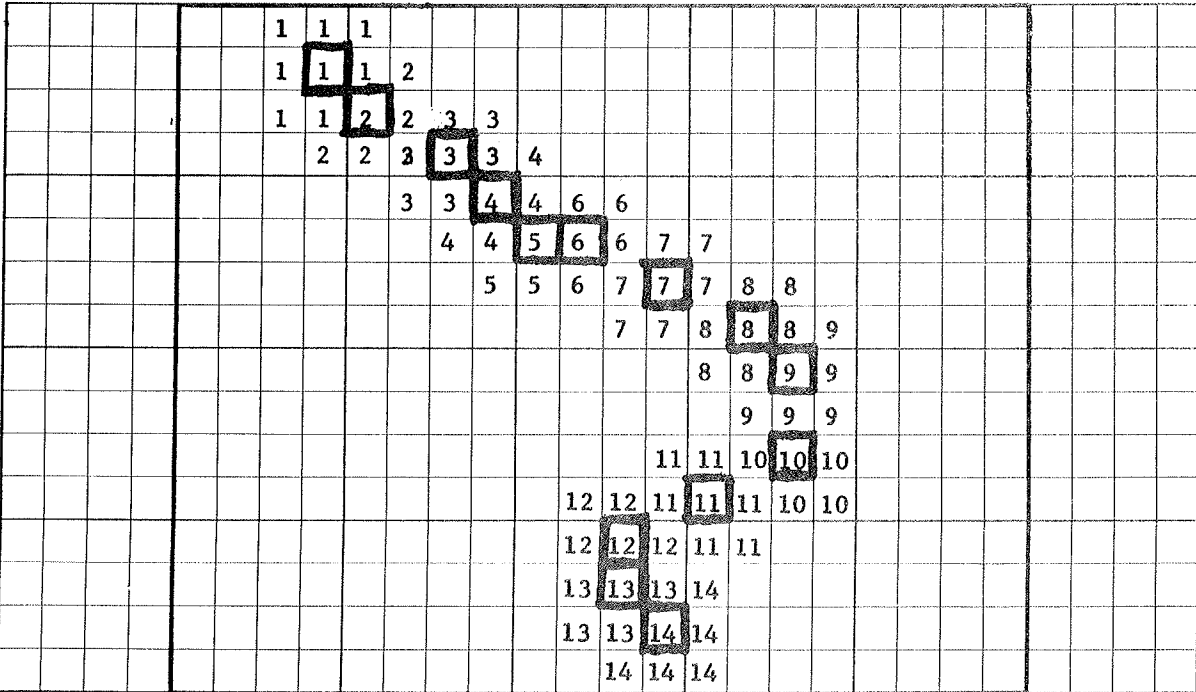


Figure 9. Automatic landmark recognition and matching procedure.

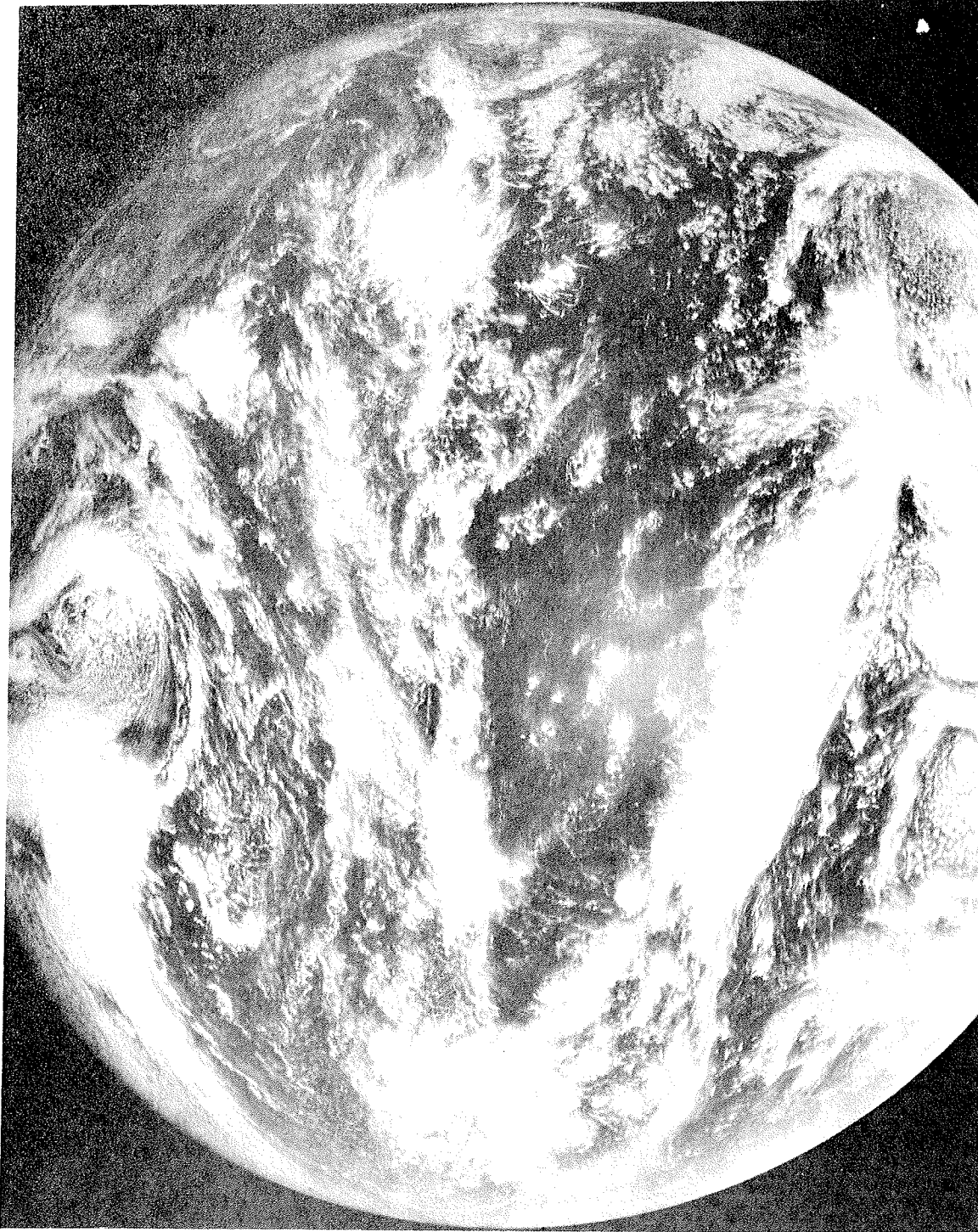


Figure 10. ATS-I sample picture displayed on the photofacsimile recorder within the Digital Picture Terminal.

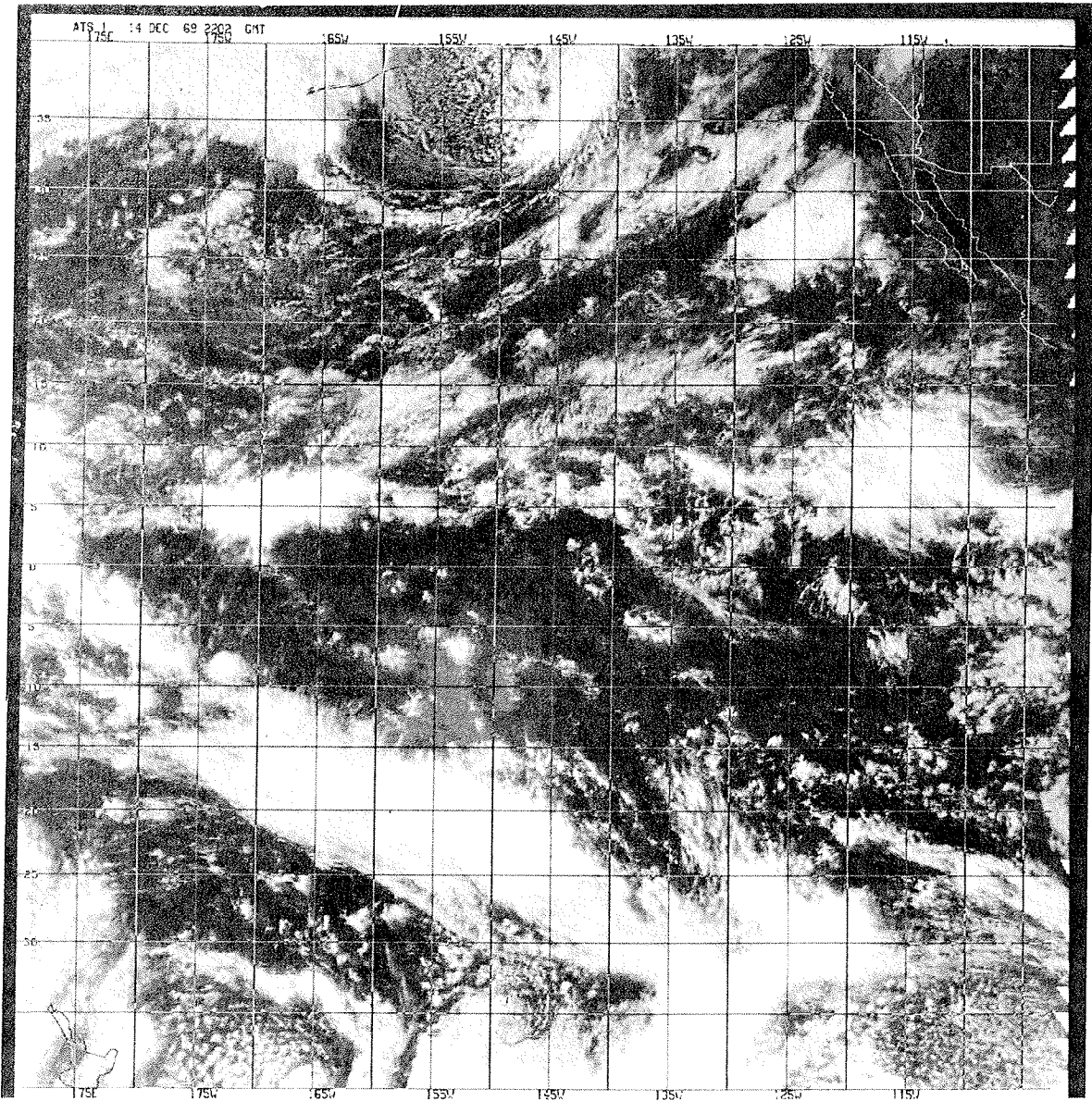


Figure 11. Mercator mapped equivalent of the picture shown in Figure 10.

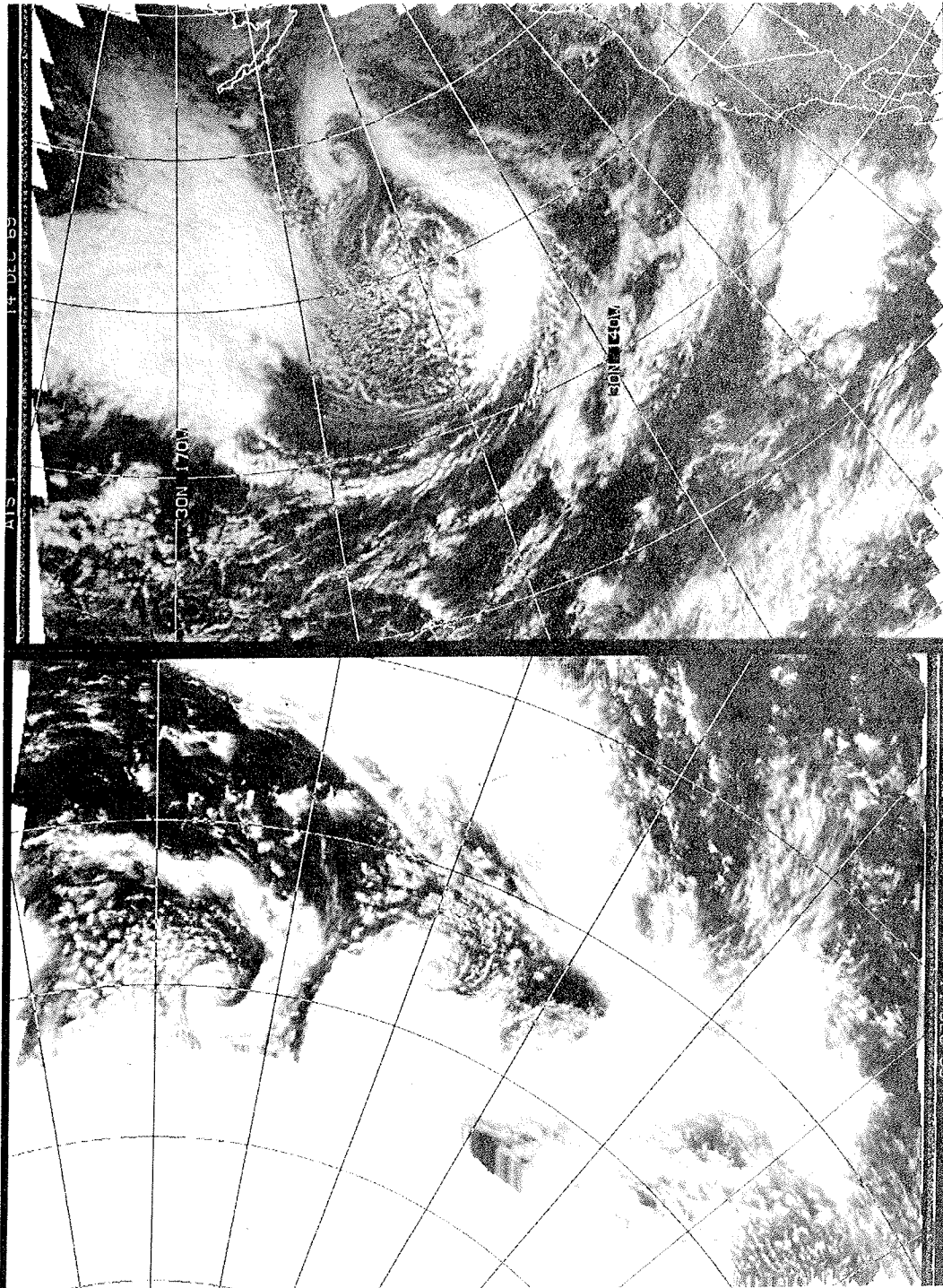


Figure 12. Polar stereographic sector images produced from Figure 10.

APPENDIX 1

Horizon Method of Attitude Determination

An observation equation is set up, for each picture line selected of the form

$$AX + BY = \text{sine}(E)$$

Where:

$$A = - \text{cosine}(\omega)$$

$$B = \text{sine}(\omega)$$

ω = satellite argument from ascending node at the time of the scan (argument of perigee + true anomaly)

$$X = \text{sine}(\text{phimax}) \cdot \text{sine}(\lambda)$$

$$Y = \text{sine}(\text{phimax}) \cdot \text{cosine}(\lambda)$$

phimax = angle between spin axis and orbit normal

λ = value of ω at which the spin axis elevation angle passes through 0° going positive (relative to subsatellite point tangent plane)

E = instantaneous elevation angle of spin axis at time of the scan line

(These equations express the roll component of the roll-yaw interchange around the orbit as used for attitude determination from V-scan data (6).)

X and Y are solved for as unknowns in two normal equations derived by the method of least squares from the observation equations, and combined to give values of phimax and λ . These in turn are converted to right ascension and declination of the spin axis vector by rotations involving the orbit inclination and right ascension of the ascending node.

Orbital elements, epoch date/time and picture start date/time are read from data cards and the time for each line is updated using the satellite

spin period. The line-by-line values of the satellite orbit phase angle (ω) are computed once per run and stored for use in successive (iterative) solutions. The spin axis elevation angle (E) for each scan line is obtained from a comparison of the observed earth sample population with tables of theoretical earth population vs scan line number which are recomputed during each iteration using the spin-axis attitude from the preceding iteration. For a spin axis fixed in inertial space, and not aligned with the normal to an inclined orbital plane, there is continuous variation of spin axis azimuth and elevation angles (referred to north, east, and up at subsatellite points) around the orbit. Changes in azimuth have no effect on the earth sample count for a spherical earth, and very little for the spheroid. On the other hand, earth sample counts for a given scan line do vary markedly with spin axis elevation angles for lines crossing the earth disk well above or below its center (see table 1).

The theoretical sample count is computed for each scan line, as follows:

a. An initial attitude is read from data cards. (For example, right ascension and declination of orbit normal - or - last previous determination of spin axis attitude.)

b. The cone-angle for the scan is computed and successive spin offsets from the mid-earth position of the telescope are assumed.

c. For each assumed position of the telescope, direction cosines are computed and projected from the satellite position to intersect the spheroid. The initial spin offset is increased by a constant increment until the radical term in the solution of a quadratic equation in slant range becomes negative, indicating that the ray no longer intersects the earth. The angular increment is then halved and the spin offset decreased until the earth is again intersected, at which time the increment is again halved and the spin increased. This iteration is continued until the tangent ray is approximated to the desired accuracy.

d. The tangent rays thus determined are projected onto a plane normal to the spin axis and the angle between them is converted to a sample count by dividing by a constant (radians/sample).

The full set of theoretical earth sample counts for the picture is scanned to find the largest, and two subtables are set up: one for the top, one for the bottom of the picture to be used as argument tables in later interpolation. Two sets of function tables are set up parallel to the argument tables - (1) the corresponding scan line number and (2) the spin axis elevation angle for that scan line computed from the assumed attitude.

For each line, L, the appropriate (top or bottom) argument table is entered with the observed earth sample count and interpolated values of computed spin axis elevation angle (E_c) and corresponding line count (L_c) are obtained.

Spin axis elevation angle is then computed as

$$E = E_c + (L - L_c) * \text{Constant} \quad (\text{radians/line change in telescope cant angle})$$

For example: Referring to table 1, if the sample count for line (-500) in column (3) is taken as an observed value and column (1) as argument table, the corresponding sample count is found at line (-600)

$$E_c = 0, \quad L_c = (-600) \quad L = (-500)$$

$$E = 0 + (-500 - (-600)) * .0075 \text{ }^\circ/\text{line} = 0.75^\circ$$

TABLE 1
Theoretical Earth Sample Counts *

Scan Line	Elev Angle=0 ^o	Elev Angle=0 ^o	Elev Angle=0.75 ^o	Elev Angle=0.75 ^o
	Azimuth =0 ^o	Azimuth=0.75 ^o	Azimuth =0 ^o	Azimuth =0.75 ^o
Top				
-1000	1791.8	1791.8	1097.7	1097.7
- 900	2240.4	2240.4	1790.4	1790.4
- 800	2575.7	2575.7	2238.9	2238.9
- 700	2838.4	2838.4	2574.2	2574.2
- 600	3047.5	3047.5	2837.0	2837.0
- 500	3213.6	3213.6	3046.2	3046.2
Center				
0	3561.7	3561.6	3548.4	3548.4
+ 500	3213.3	3213.3	3344.4	3344.4
+ 600	3047.1	3047.1	3214.9	3214.9
+ 700	2837.9	2837.9	3048.9	3048.9
+ 800	2575.0	2575.0	2839.8	2839.8
+ 900	2239.5	2239.5	2577.0	2577.0
Bottom				
+1000	1790.6	1790.6	2241.4	2241.4

* Computed for a subsatellite point latitude at 1^o north, height 35,800 km, Radians-per-line 0.0001309, Radians-per-sample 0.000085242.

In order to obtain accuracy with this method, it is necessary to exclude scan lines near the center of the disk where the earth sample population is insensitive to changes in spin axis elevation angle, and to include in the solution scans at both top and bottom so as to make use of information from as large a portion of the orbit as possible within the confines of a single picture.

The program computes the sun elevation angle at each theoretical horizon point and flags those where illumination is insufficient. The corresponding observed earth-edge data are not used in the solution for that iteration. To extend the range of lines used in the solution, for pictures in which only one or the other horizon is in sunlight at the greater north and south latitudes, it is necessary to determine earth populations from a single horizon. To permit this, the program logic includes a least-squares solution for the mid-earth sample number at the top of the picture, and a straight line slope of mid-earth position from top to bottom, which best fits all of the illuminated earth edge points. (This assumed straight-line drift approximates small errors in spin phase resulting from imperfect setting of the "beta dot" value which controls the line synchronism.) Accuracy in attitude determination also requires a precise knowledge of the radians-per-sample constant used in converting rotations about the spin axis to theoretical earth sample counts. The least squares solution for the mid-earth line also computes a value for this constant which will minimize the line-to-line differences between observed and theoretical earth populations.

The radians-per-line constant could be more simply computed as the ratio of radians-per-second (obtained from the satellite spin rate RPM) to the samples-per-second digitizing rate. Lacking precise information on the A/D converter rate, recourse was made to the least squares solution mentioned above, and also determined empirically from the mid-earth-disk sample population and the corresponding angle at the satellite between tangent rays to the left and right horizons. For the ATS-I satellite, at a distance of 42167 kilometers from the center of the earth,¹ this angle is 0.30373 radians, and an average earth population obtained from 20 pictures, with the threshold at 16, is 3786 samples. Use of a lower threshold would increase this number. (For one picture a difference of 16 samples was observed between thresholds of 8 and 16.) The ratio of 0.30373 radians to 3800 samples gives a value for the constant of 79.93 microradians-per-sample. This value is in fair agreement with that which would be obtained for the current ATS-I spin rate of 93.5 RPM with the A/D conversion set to represent 20° of spin rotation at 100 RPM by 4096 samples. (79.68 microradians-per-sample and an earth sample population of 3812.) The program currently uses an input value of 80.0 microradians-per-sample with an option to use the empirically determined values, if desired.

¹ An average value for the semimajor axis determined from 10 sets of orbital elements is very nearly 42167 kilometers with variations not exceeding 2 kilometers. Variations in earth-satellite distance around the orbit, which has an eccentricity on the order of 0.0003, is on the order of ± 12 kilometers.

Operational testing of the method was carried out on an almost daily basis between June 11 and July 20, and for one week in August and another in September. Currently, it is being run only on weekends. The earlier attitude determinations were generally of low accuracy as various program flaws were uncovered. Table 2 contains a representative list of the better determinations as an indication of the potential of the method. Table 3 lists the results of the least square solution for the mid-earth line and the angular increment per sample. The "initial" spin given in Table 2 is computed for the first scan line of a picture using the data from Table 3, and equals 2048 minus the mid-earth sample number, all multiplied by microradians per sample, converted to degrees. The per-line change in spin is computed in a similar manner and represents a spin phase drift over a picture ranging from 0.03 to 0.2 degrees. Three accuracy indicators are included in table 2. The standard deviation column lists the one-standard deviation (one-sigma) errors for the sine of the elevation angle, in the solution to the basic observation equations. The "sample delta" column shows the root mean-square average difference between the observed and theoretical earth population sample counts. The "CCA ERROR" is the great circle arc equivalent of the one-sigma errors in right ascension and declination of the spin axis vector.

TABLE 2

Date 1969	Time (GCT)	Spin Axis Attitude (Degrees)		Spin (Degrees) Initial	Change per Line (Times 10 ⁻⁵)	Standard Deviation	Sample Delta	GCA Error (Degrees)
		R.A.	Decl.					
6/29	2149	332.65±.05	87.16±.02	0.344	-4.85	.00047	22.6	.025
7/20	2131	349.01±.30	88.04±.02	-0.079	-6.09	.00041	4.96	.021
7/31	2142	345.80±.21	88.17±.01	-0.153	-4.135	.00022	3.19	.011
8/ 1	2147	346.17±.01	88.16±.001	0.168	-3.525	.00024	3.02	.001
8/ 2	2126	346.32±.01	88.17±.001	0.079	-6.225	.00026	3.03	.001
8/ 6	2128	352.47±.86	88.10±.03	0.239	-6.790	.00068	109.5	.039
8/18	2132	324.51±.19	88.41±.01	-0.021	-1.483	.00020	23.5	.010
8/20	2130	320.64±.17	88.40±.01	0.002	-2.876	.00019	5.49	.009
9/ 6	2131	346.47±.49	88.21±.004	0.077	-2.423	.00034	6.19	.016
9/ 9	2144	350.13±.92	88.14±.003	0.187	-2.202	.00029	6.18	.014
9/12	2139	352.82±.41	88.13±.002	0.143	-3.289	.00028	5.53	.013
9/15	2132	351.00±.30	88.06±.001	0.012	-3.805	.00021	4.68	.010
9/21	2136	348.34±.33	88.09±.002	0.202	-7.058	.00021	4.10	.011
10/ 7	2140	348.72±.21	87.85±.004	0.268	-10.093	.00016	3.01	.009
10/10	2133	345.61±.17	87.78±.004	0.550	-9.991	.00015	8.19	.008
10/19	2136	333.17±.14	86.96±.01	0.171	-5.844	.00024	4.07	.012
10/26	2130	20.37±.34	88.15±.01	0.306	-5.538	.00020	4.18	.011
11/ 2	2119	14.89±.31	87.67±.01	0.302	-3.578	.00025	4.92	.013
11/ 5	2124	350.37±.22	86.81±.01	0.035	-4.483	.00036	7.36	.019
12/30	2150	301.83±.74	88.91±.09	0.199	-10.934	.00029	5.53	.029
1/ 9	2136	265.68±.81	88.85±.06	-0.027	-7.087	.00027	6.53	.019
1/14	2132	268.90±.78	88.83±.06	0.024	-5.322	.00033	6.53	.020
1/17	2129	257.33±.68	88.73±.05	0.059	-10.377	.00030	9.94	.017

TABLE 3

Date 1969	Time (GCT)	Midearth (Midhorizon) Line First Scan Sample Number	(Samples per Line) Slope Times 10^{-3}	Microradians per Sample
6/29	2149	1973.25 \pm .28	10.99 \pm .21	80.055
7/20	2131	2064.63 \pm .24	13.28 \pm .17	80.058
7/31	2142	2080.99 \pm .22	9.02 \pm .16	79.991
8/ 1	2147	2010.85 \pm .28	7.69 \pm .20	80.011
8/ 2	2126	2030.31 \pm .22	13.59 \pm .16	79.980
8/ 6	2128	1995.49 \pm .54	14.79 \pm .43	80.095
8/18	2132	2052.20 \pm .18	3.24 \pm .13	79.804
8/20	2130	2047.95 \pm .19	6.29 \pm .14	79.750
9/ 6	2131	2030.71 \pm .30	5.30 \pm .02	79.859
9/ 9	2144	2006.79 \pm .33	4.81 \pm .24	79.976
9/12	2139	2016.32 \pm .32	7.18 \pm .24	79.895
9/15	2132	2044.83 \pm .33	8.30 \pm .30	79.990
9/21	2136	2012.51 \pm .44	9.42 \pm .32	80.044
10/ 7	2140	1982.93 \pm .22	26.92 \pm .16	80.080
10/10	2133	1922.72 \pm .22	25.48 \pm .15	80.050
10/19	2136	2012.59 \pm .34	9.92 \pm .25	79.787
10/26	2130	1978.14 \pm .18	14.08 \pm .14	80.218
11/ 2	2119	1978.15 \pm .24	8.52 \pm .19	80.190
11/ 5	2124	2037.33 \pm .23	13.11 \pm .18	79.848
12/30	2150	2006.58 \pm .58	24.08 \pm .39	79.943
1/ 9	2136	2056.66 \pm .20	14.06 \pm .12	79.862
1/14	2132	2042.35 \pm .24	12.81 \pm .15	79.827
1/17	2129	2051.14 \pm .29	13.37 \pm .18	80.210

APPENDIX 2

Attitude Calculation with the Landmark Method

Using two or more landmarks, attitude can be calculated by minimizing the square of the difference of direction cosines for rays from the satellite to landmarks as determined from the observed image position, and from the image position computed using the estimated attitude. The ray directions corresponding to the two sets of images are first converted to unit vectors ("observed" and "computed"). By multiplying the computed vector by a rotational matrix and subtracting the observed vector, an error vector is obtained. The squares of the three components of the error vector are added to obtain a function of the three rotation angles. The functions thus obtained for each landmark are combined to form a composite function of the attitude. The function can be minimized by finding the point where it has a zero slope.

Let $B(\alpha, \beta, \gamma)$ be the rotational matrix, where α is the yaw angle, β is the roll angle, and γ is the pitch angle.

$$B = \begin{bmatrix} \cos \beta \cos \gamma & \cos \beta \sin \gamma & \sin \beta \\ -\sin \beta \sin \alpha \cos \gamma - \cos \alpha \sin \gamma & -\sin \beta \sin \alpha \sin \gamma + \cos \alpha \cos \gamma & \cos \beta \sin \alpha \\ -\sin \beta \cos \alpha \cos \gamma + \sin \alpha \sin \gamma & -\sin \beta \cos \alpha \sin \gamma - \cos \alpha \sin \gamma & \cos \beta \cos \alpha \end{bmatrix}$$

Let B_{ij} be an element of B: $i = \text{column}$ $j = \text{row}$
 If E is the unit vector of a known landmark, then let E_{jk} be an element of the K^{th} landmark

$j = \text{the axis number of the vector.}$

Let P_{ik} be an element of the unit vector of the K^{th} observed landmark P.

$i = \text{the axis number of the vector.}$

If we rotate each element of E by B and subtract P the result will be an error residual.

$$\sum_{j=1}^3 B_{ij} \cdot E_{jk} - P_{ik} = \text{error}$$

If we sum the squares of the residuals for each element of the unit vectors for each landmark we get a function of α, β, γ

$$\sum_{k=1}^M \left[\sum_{i=1}^3 \left(\sum_{j=1}^3 B_{ij} E_{jk} - P_{ki} \right)^2 \right] = F(\alpha, \beta, \gamma)$$

where M is the number of landmarks.

If we expand this we get

$$\begin{aligned} & \sum_{K=1}^M \left[\sum_{i=1}^3 (B_{i1} E_{1K} + B_{i2} E_{2K} + B_{i3} E_{3K} - P_{Ki})^2 \right] \\ &= \sum_{K=1}^M \left[\sum_{i=1}^3 (B_{i1}^2 E_{1K}^2 + B_{i2}^2 E_{2K}^2 + B_{i3}^2 E_{3K}^2 + 2 B_{i1} B_{i2} E_{1K} E_{2K} \right. \\ & \quad \left. + 2 B_{i2} B_{i3} E_{2K} E_{3K} + 2 \{ B_{i1} E_{1K} + B_{i2} E_{2K} \right. \\ & \quad \left. + B_{i3} E_{3K} \} P_{Ki} + P_{Ki}^2) \right] \end{aligned}$$

Since B is a rotational matrix $\sum_{i=1}^3 B_{ik} B_{ik} = 1$,

and $\sum_{i=1}^3 B_{ik} B_{ij} = 0$ ($j \neq k$).

Then $\sum_{i=1}^3 (B_{i1}^2 E_{1K}^2 + B_{i2}^2 E_{2K}^2 + B_{i3}^2 E_{3K}^2) = E_{1K}^2 + E_{2K}^2 + E_{3K}^2$,

and $\sum_{i=1}^3 2[(B_{i1} B_{i2}) E_{1K} E_{2K} + (B_{i1} B_{i3}) E_{1K} E_{3K} + (B_{i2} B_{i3}) E_{2K} E_{3K}] = 0$.

Then F becomes

$$F = \sum_{K=1}^M \left[2 \sum_{i=1}^3 \left\{ (B_{i1} E_{1K} + B_{i2} E_{2K} + B_{i3} E_{3K}) P_{Ki} \right\} + C_K \right]$$

where C_K is a constant equal to $E_{1K}^2 + E_{2K}^2 + E_{3K}^2 + P_{K1}^2 + P_{K2}^2 + P_{K3}^2$

Since we are only concerned with where F becomes a minimum, the constants can be ignored.

If $F' = \begin{bmatrix} F_1 & 0 & 0 \\ 0 & F_2 & 0 \\ 0 & 0 & F_3 \end{bmatrix}$, and $F = F_1 + F_2 + F_3$,

Then F' becomes the matrix multiplication

$$F' = (BE)P \text{ which equals } B(EP)$$

$$\text{and if } R = EP, \quad F'(\alpha, \beta, \gamma) = B(\alpha, \beta, \gamma) \cdot R,$$

where R is a constant matrix.

The point where F has a minimum is found by adjusting an initial value of α, β, γ by the negative gradient of F . This process is continued until the gradient approaches a level close to zero.

$$\alpha_{i+1} = \alpha_i - a \frac{\partial F}{\partial \alpha} ,$$

$$\beta_{i+1} = \beta_i - a \frac{\partial F}{\partial \beta} ,$$

$$\gamma_{i+1} = \gamma_i - a \frac{\partial F}{\partial \gamma} ,$$

where a = a weighting factor for the gradient to prevent over correction.

The values of roll and yaw thus computed are converted into right ascension and declination of a geocentric vector parallel to the spin axis. The pitch angle represents rotation about the spin axis.

(Continued from inside front cover)

- NESCTM 11 Publications by Staff Members, National Environmental Satellite Center and Final Reports on Contracts and Grants Sponsored by the National Environmental Satellite Center 1968. January 1969. (PB-182 853)
- NESCTM 12 Experimental Large-Scale Snow and Ice Mapping With Composite Minimum Brightness Charts. E. Paul McClain and Donald R. Baker, September 1969. (PB-186 362)
- NESCTM 13 Deriving Upper Tropospheric Winds by Computer From Single Image, Digital Satellite Data. Charles S. Novak, June 1969. (PB-185 086)
- NESCTM 14 Reserved.
- NESCTM 15 Some Aspects of the Vorticity Structure Associated With Extratropical Cloud Systems. Harold J. Brodrick, Jr., May 1969. (PB-184 178)
- NESCTM 16 The Improvement of Clear Column Radiance Determination With a Supplementary 3.8μ Window Channel. William L. Smith, July 1969. (PB-185 065)
- NESCTM 17 Vidicon Data Limitations. Arthur Schwalb and James Gross, June 1969. (PB-185 966)
- NESCTM 18 On the Statistical Relation Between Geopotential Height and Temperature-Pressure Profiles. W. L. Smith and S. Fritz, November 1969. (PB-189 276)
- NESCTM 19 Applications of Environmental Satellite Data to Oceanography and Hydrology. E. Paul McClain, January 1970.

